PHILOSOPHICAL TRANSACTIONS A

rsta.royalsocietypublishing.org

Research

Cite this article: Van Renterghem T. 2017 Sound propagation from a ridge wind turbine across a valley. *Phil. Trans. R. Soc. A* **375**: 20160105.
http://dx.doi.org/10.1098/rsta.2016.0105

Received: 17 June 2016
Accepted: 29 September 2016

One contribution of 11 to a theme issue 'Wind energy in complex terrains'.

Subject Areas:
computational physics, atmospheric science, environmental engineering, acoustics

Keywords:
outdoor sound propagation, wind turbine, undulating terrain, parabolic equation method

Author for correspondence:
Timothy Van Renterghem
e-mail: timothy.vanrenterghem@ugent.be

Sound propagation from a ridge wind turbine across a valley

Timothy Van Renterghem

Department of Information Technology, Ghent University, iGent tower, Technologiepark 15, 9052 Zwijnaarde, Belgium

TVR, 0000-0003-0435-5485

Sound propagation outdoors can be strongly affected by ground topography. The existence of hills and valleys between a source and receiver can lead to the shielding or focusing of sound waves. Such effects can result in significant variations in received sound levels. In addition, wind speed and air temperature gradients in the atmospheric boundary layer also play an important role. All of the foregoing factors can become especially important for the case of wind turbines located on a ridge overlooking a valley. Ridges are often selected for wind turbines in order to increase their energy capture potential through the wind speed-up effects often experienced in such locations. In this paper, a hybrid calculation method is presented to model such a case, relying on an analytical solution for sound diffraction around an impedance cylinder and the conformal mapping (CM) Green's function parabolic equation (GFPE) technique. The various aspects of the model have been successfully validated against alternative prediction methods. Example calculations with this hybrid analytical–CM–GFPE model show the complex sound pressure level distribution across the valley and the effect of valley ground type. The proposed method has the potential to include the effect of refraction through the inclusion of complex wind and temperature fields, although this aspect has been highly simplified in the current simulations.

This article is part of the themed issue 'Wind energy in complex terrains'.

1. Introduction

In order to fulfil the renewable energy targets that have been set in many countries, the number of wind turbines

THE ROYAL SOCIETY PUBLISHING

is expected to increase significantly in the near future. Among the different environmental impacts associated with wind turbines (such as landscape and visual impact, shadow flicker, impact on wildlife, electromagnetic interference and climate change [1]), noise issues remain the key environmental factor controlling the extent of a wind farm's development [2]. Even at low A-weighted sound pressure levels, there is a substantial negative perception towards wind turbine noise [3–8]. Therefore, noise impact assessments are commonly required during the planning phase.

Positioning wind turbines on ridges can potentially intensify momentum extraction from the wind flow [9], caused by the so-called wind speed-up effect [10–12]. Parameters of relevance include hill shape, the terrain upwind of the hill, atmospheric stability and whether or not the hill is forested [9–12].

However, there is little research, to the author's knowledge, regarding sound propagation from a ridge-mounted wind turbine to receptor locations across an adjacent valley, although the measurement-based studies of Evans & Cooper [13] have highlighted the importance of topography, including valleys, for wind turbine noise propagation. Established knowledge from other types of environmental noise sources cannot be easily transferred to the present case due to the unique positioning of the source high above a ridge. Physical phenomena that could be relevant to the present case include amplification of sound due to the valley (potentially mediated or intensified by the valley shape and its acoustic ground impedance), partial shielding by the ridge, and atmospheric refraction and turbulent scattering of sound waves due to the complex flow fields that are expected in such a geometry. Both the hilly topography and the presence of a turbine will add to the complexity of the flow. In this work, some of these aspects are studied by means of numerical sound propagation modelling.

Study of the foregoing expected sound propagation effects demands an advanced outdoor sound propagation technique. However, consideration additionally needs to be given to the computational cost, and therefore also the practical applicability of any such advanced techniques. Meta-analysis of (perception) studies with regard to wind turbine noise annoyance [14] state that, below 35 dBA, negative effects are generally not found. Logically, the latter defines the distance of concern. For large horizontal-axis wind turbines, with total source power levels easily exceeding 100 dBA when operating near their maximum power production, a propagation distance of minimum 1 km from the source should be attained. Knowing that wind turbine noise emission spectra typically show a maximum near the octave band of 1 kHz [15,16], and given that sufficiently detailed wave propagation techniques need sub-wavelength discretization, the numerical problem becomes challenging regarding spatio-temporal discretization.

An interesting candidate is the parabolic equation (PE) method (see e.g. [17,18]). The simplification to one-way sound propagation allows efficient solving of the governing sound propagation equations. In addition, a refracting atmosphere can be accounted for in detail. For many cases involving long-distance sound propagation, reasonably accurate predictions can be made with this methodology. Of specific interest is the Green's function parabolic equation (GFPE) method [19,20], as this allows forward stepping at multiples of the wavelength, in contrast to the sub-wavelength step spacing of most other advanced techniques.

The GFPE, however, cannot be readily used to model sound propagation from a ridge-mounted wind turbine. The inclusion of undulating terrain will be discussed in this work, and a number of specific problems will be dealt with. Focus is on accurately accounting for the effect of terrain undulation in the case of a source positioned high above a ridge. In addition, some example calculations are provided to show the potential of the proposed model.

In this paper, the specific wind and temperature fields near a ridge wind turbine are not considered. Only a highly simplified approach is used to model downwind sound propagation, although more complex flow fields could be rather easily included in the GFPE methodology. Turbulence scattering and coherence loss are also not considered in this work. Note that, although there is strong progress in computational fluid dynamics modelling, providing detailed flow fields in the case of a ridge-mounted wind turbine still remains highly challenging.

2. The Green's function parabolic equation method in undulating terrain

(a) Basic stepping equation

The two-dimensional stepping equation of the GFPE method is summarized by equation (2.1). Some basic features of this technique are discussed below, but a detailed derivation and analysis can be found elsewhere [17,19,20]. In this forward propagation approach, the vertical array of pressures p at range $r + \mathrm{d}r$ is extrapolated from the previous column at range r. Thus

$$p(r+\mathrm{d}r,z) = \exp(-\mathrm{i}\mathrm{d}r k_0)\overbrace{\exp(\mathrm{i}\mathrm{d}r(k-k_0))}^{\text{refraction term}} \times \overbrace{\left\{\frac{1}{2\pi}\int_{-\infty}^{\infty}\exp\left(\mathrm{i}\mathrm{d}r\sqrt{k_0^2-k_z^2}\right)\exp(\mathrm{i}k_z z)\,\mathrm{d}k_z\int_0^{\infty}\exp(-\mathrm{i}k_z z')p(r,z')\,\mathrm{d}z'\right.}^{\text{direct wave}} + \overbrace{\frac{1}{2\pi}\int_{-\infty}^{\infty}R(k_z)\exp\left(\mathrm{i}\mathrm{d}r\sqrt{k_0^2-k_z^2}\right)\exp(\mathrm{i}k_z z)\,\mathrm{d}k_z\int_0^{\infty}\exp(\mathrm{i}k_z z')p(r,z')\,\mathrm{d}z'}^{\text{ground-reflected wave}} + \overbrace{\left.2\mathrm{i}\frac{k_0}{Z}\exp\left(-\mathrm{i}\frac{k_0}{Z}z\right)\exp\left(\mathrm{i}\mathrm{d}r\sqrt{k_0^2-(k_0/Z)^2}\right)\int_0^{\infty}\exp\left(-\mathrm{i}\frac{k_0}{Z}z'\right)p(r,z')\,\mathrm{d}z'\right\}}^{\text{surface wave}}, \quad (2.1)$$

with i the imaginary unit, (r, z) the position in, respectively, the horizontal and vertical direction with $\mathrm{d}r$ and $\mathrm{d}z$ their spatial discretization steps, Z the ground impedance normalized to that of (unbounded) air ($=\rho_0 c_0$, with ρ_0 the mass density of air and c_0 the sound speed; local reaction approximation), k_0 the reference wavenumber (at the ground surface), k the height-dependent wavenumber ($k = 2\pi f/c$, with f the sound frequency under consideration) and k_z the wavenumber in the (vertical) spatial (Fourier) domain.

Some distinct contributions in equation (2.1) can be identified, namely the direct wave, the ground-reflected wave and a surface wave. Refraction can be efficiently approached by a phase correction due to wavenumber variations with height. Temperature (and to a lesser extent humidity) variations with height are directly linked to changes in sound speed [17,18] involving no approximations. The horizontal components of the wind speed (parallel to the ground) can be approached by an equivalent increase in the sound speed (i.e. the so-called 'effective sound speed' approach [17,18]). This stepwise calculation of the acoustic fields allows both the sound speed profile and the ground parameters to be made range-dependent.

The integrals appearing in the direct and ground-reflected wave terms can be efficiently calculated by relying on the Fourier transform and its inverse, for which numerically very efficient algorithms are commonly available, such as the fast Fourier transform.

In order to represent the wind turbine noise source as a point source, the calculations will rely on the equivalence between (coherent) line source propagation (i.e. the two-dimensional solution) and point source propagation (i.e. the three-dimensional solution) when expressing sound pressure levels relative to free-field sound propagation [21] (see §4).

(b) Including terrain undulations

Various approaches for introducing undulating terrain in the PE method can be found, like the general terrain PE (GTPE) [22], the rotated reference frame approach [23–25] (GFrPE), a stair-step terrain approach using Kirchoff's method [26] and the conformal mapping (CM) method [17,27,28].

The GTPE can be seen as a generalization of the Crank–Nicolson PE (CNPE) method. This method is applicable to arbitrary terrain profiles and uses terrain-following coordinates. However, analysis has shown that the local slope angles should not exceed roughly 30° [17].

In addition, the CNPE is much less efficient than the GFPE, as stepping in the propagation direction needs sub-wavelength discretization.

The rotated reference frame approach is applicable to the GFPE. The curved ground is treated as a succession of flat zones with different slope angles. The sound field in each domain starts from an array of pressure values, orthogonal to the local slope, as calculated from the previous domain. A number of reduced propagation steps are thus needed near the interface to accurately construct the next domain's starting field, which can strongly increase computing times [25]. Sudden slope changes along the propagation path are difficult to handle.

The stair-step approach might be attractive due to its simplicity. The terrain profile is reduced to a succession of best-fitting steps that are each treated as small vertical barriers. The part of the sound field covered by each step is then set to zero. This method further needs a vertical coordinate shift to continue propagation from the top of the next step. Combining the foregoing approach with variable step widths provides great flexibility in describing terrain profiles. However, only reflection on horizontal surfaces is modelled. This means that waves reflected obliquely in the direction of sound propagation cannot subsequently interfere along the propagation path. Only part of the acoustic energy will be sent in that direction due to diffraction at step corners, thereby potentially resulting in a significant loss in accuracy.

In this study, the CM method will be used, which is a computationally highly efficient approach to account for undulating terrain. The CM method is based on the theoretically perfect analogy between a circularly curved ground surface with radius R_c and a refracting atmosphere with the following exponential sound speed profile c:

$$c = c_0 e^{z/R_c}, \tag{2.2}$$

with $R_c > 0$ for concave ground and $R_c < 0$ for convex ground, z the height above the ground and c_0 the reference sound speed.

The shielding caused by convex terrain can thus be approached by sound propagating over flat terrain in an upwardly refracting atmosphere, while concave ground is simulated by a downwardly refracting atmosphere. A change in sound speed profile comes at almost no additional computational cost in the PE model. Note that such artificially refracting atmospheres due to ground curvature are typically much stronger than those observed due to real wind flows in the atmospheric boundary layer. The latter, however, can be superimposed on the artificial profile due to ground curving, thus allowing account to be taken of both terrain undulation and atmospheric refraction.

The main limitation here is the need for simplification to circularly curved terrain segments. Care is needed to account for the coordinate transform between the real (curved ground) system and the artificially refractive flat PE domain.

3. Hybrid analytical–conformal mapping–Green's function parabolic equation model

When applying the GFPE to the specific case of sound propagation across a valley from a ridge-mounted wind turbine, two fundamental problems appear.

Firstly, a direct application of the CM approach would actually mean that the source becomes oriented perpendicular to the curved ground. Clearly, such a configuration, as schematically illustrated in figure 1*a*, deviates strongly from a typical wind turbine case. A more realistic scenario, still consistent with the CM approach, can be achieved by placing two circular ground segments in series [17,27] (figure 1*b*). The geometry of interest is thus idealized to sound propagation over a small convex circular segment representing the ridge (with artificial upward refraction), followed by sound propagation over part of a large concave cylinder representing the valley (with artificial downward refraction).

A second fundamental problem when using the PE method for such a case is that sound propagation can only be accurately described in a relative small cone, horizontally centred around

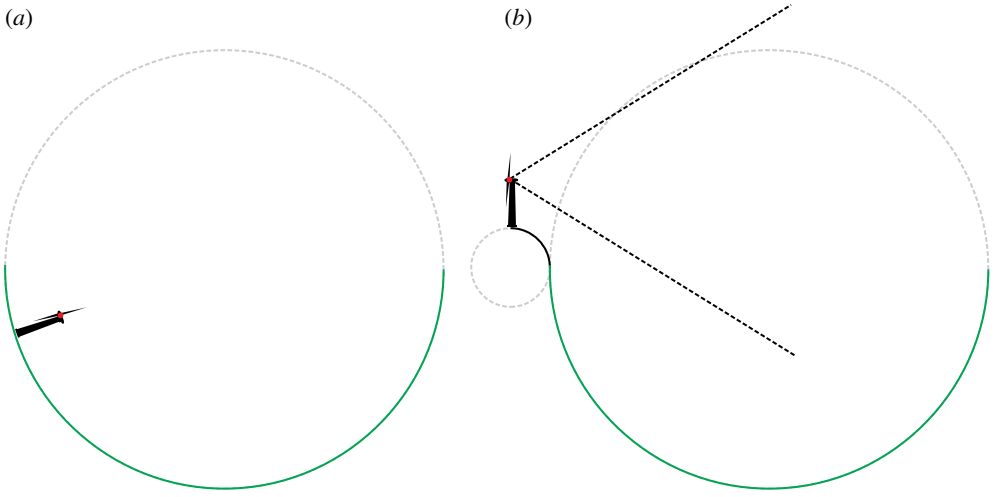

Figure 1. Schematics of two fundamental problems associated with CM–GFPE modelling applied to sound propagation from a ridge wind turbine. (Online version in colour.)

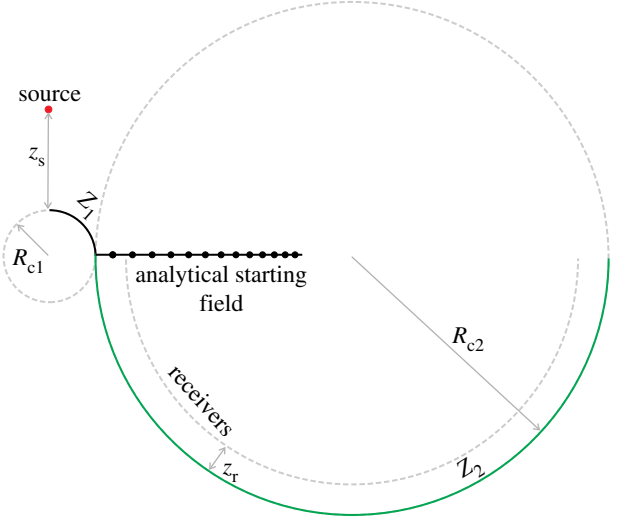

Figure 2. Geometry of the hybrid analytical–CM–GFPE model for simulating sound propagation from an elevated sound source, positioned at a ridge (radius R_{c1}, source height z_s), towards a valley (radius R_{c2}, receiver heights z_r). Z_1 and Z_2 are the ground impedances of the ridge and valley parts, respectively. (Online version in colour.)

the source. In the current context with a source at a large height, a major part of the valley would be artificially put in an acoustic shadow zone (figure 1*b*), leading to inaccurate results. Although applying a higher-order source approximation could extend the cone with correct predictions [17], at the source side of the valley this problem would still remain.

The solution to this problem is found in the fact that the GFPE method is able to commence from any vertical array of pressures that can be accurately calculated at sub-wavelength spacing. There are actually three possibilities. Most commonly used is a Gaussian starter [17] as the first column of pressures, representing a monopole source. Accuracy up to larger propagation angles can be achieved by a higher-order approach of the latter [17]. Secondly, another full-wave technique can be used to produce a starting field at close distance from the source [21,29]. A third

option, as done in this work, uses the analytical solution for coherent line source diffraction around an impedance cylinder (with circular cross-section), with the line source parallel to the cylinder axis (summarized in appendix A).

As a result, the current hybrid analytical–CM–GFPE model does not suffer from angle limitations in the source region. As shown in figure 2, sound propagation over exactly one-quarter of the cylinder, representing the ridge, is simulated to facilitate the coupling to the valley part. This avoids complicated interpolation at the interface with the valley section. Note that, for the valley part, the ground can be further split up in segments with different impedance. The starting field must be characterized on a vertical grid with a (logarithmically) decreasing spacing towards higher positions. This is necessary to comply with the CM coordinate transform from the curved surface to a grid with a uniform vertical spacing in an (artificially) refracting environment [17,27].

4. Numerical validation

The numerical codes and their parameter choices employed in this study have been validated in two-dimensional cases by intercomparison with other prediction methods (see figure 3 and table 1 for an overview). Note that, although the numerical techniques proposed for the hybrid model (see §3) are theoretically sound, such an exercise is still useful: it is stressed, e.g. in [30], that the GFPE method needs some critical parameter choices, potentially strongly impacting on numerical accuracy. All surfaces were chosen to be rigid, allowing a detailed check of the accuracy of predicted interferences, these becoming most pronounced in such a case. Sound pressure levels relative to free-field propagation (unbounded domain) are compared in all cases. This allows focus to be maintained on the physical wave aspects since geometrical divergence, which is always present, is excluded.

In case A, the axisymmetric [17] CM–GFPE is validated against the analytical solution for sound diffraction around a cylinder (see appendix A) in the case of circularly convex ground. Note that the CM–GFPE could give rise to numerical issues when source and/or receiver heights are large relative to the ground radius [17]. Therefore, a somewhat larger radius was chosen than would otherwise be appropriate for the ridge part of the model.

In case B, the axisymmetric CM–GFPE is compared with the two-dimensional finite-difference time-domain (FDTD) technique [31] for the case of a circularly concave ground segment. The FDTD technique can be considered as a reference solution over a wide range of acoustical applications. A somewhat larger radius for the ground curvature is now taken compared with validation case A, but still smaller than the radius of a typical valley. This is because the FDTD method is computationally highly demanding. Note that the effect of ground curvature on sound propagation becomes visible at a short distance (see later), thereby justifying this choice. The FDTD code as used here, in its basic form, employs a staircase approach, leading to scattering at the rigid edges of the steps. This effect can be strongly reduced when analysing a lower sound frequency, ensuring a high ratio between wavelength and spatial discretization step.

In case C, the methodology to develop the GFPE solution from an analytically constructed, coherent line source starting field is compared with the analytical solution of sound propagation over flat rigid ground, directly starting from the source. A two-ray analytical solution for a coherent line source is used for the latter [17,32,33].

Validation case A shows good agreement between the analytical solution describing sound propagating around a circular rigid cylinder and the CM–GFPE. Figure 4 shows the sound field in the transformed coordinate system used by the CM–GFPE (with r the distance along the arc). Receivers are positioned at a fixed height relative to the arc. At close distance, the angle limitation of the PE method becomes visible, as discussed before. Note that an eighth-order starting field was used here (see §3 and [17]), thereby partly mitigating this inaccuracy. The CM–GFPE yields somewhat less pronounced destructive interference dips that appear at short distance in this particular case; the (very) low levels due to sound wave cancelling are typically not reached with a numerical technique. Near the constructive interferences, differences amount to 0.6 dB. In the deep shadow zone, some small oscillations in the CM–GFPE could be observed.

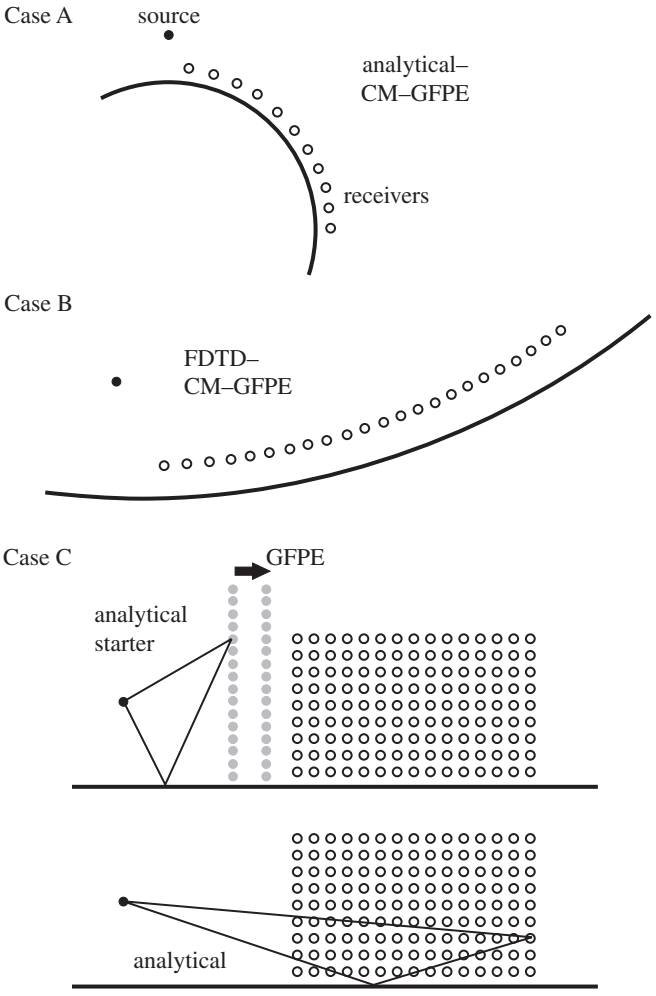

Figure 3. Schematics of the validation cases considered.

Table 1. Cross-validation cases considered, with indication of their geometries.

parameter	case A	case B	case C
models compared	CM–GFPE versus analytical solution	CM–GFPE versus FDTD	GFPE with analytical starter versus (full) analytical solution
sound frequency (Hz)	500	250	500
R_c (m)	−50 (convex)	100 (concave)	∞ (flat)
z_s (m)	5	5	5
z_r (m)	1	2	zone of receivers
maximum angle over which propagated	$\pi/2$	$\pi/6$	zone of receivers
maximum propagation distance along arc (m)	78	50	550

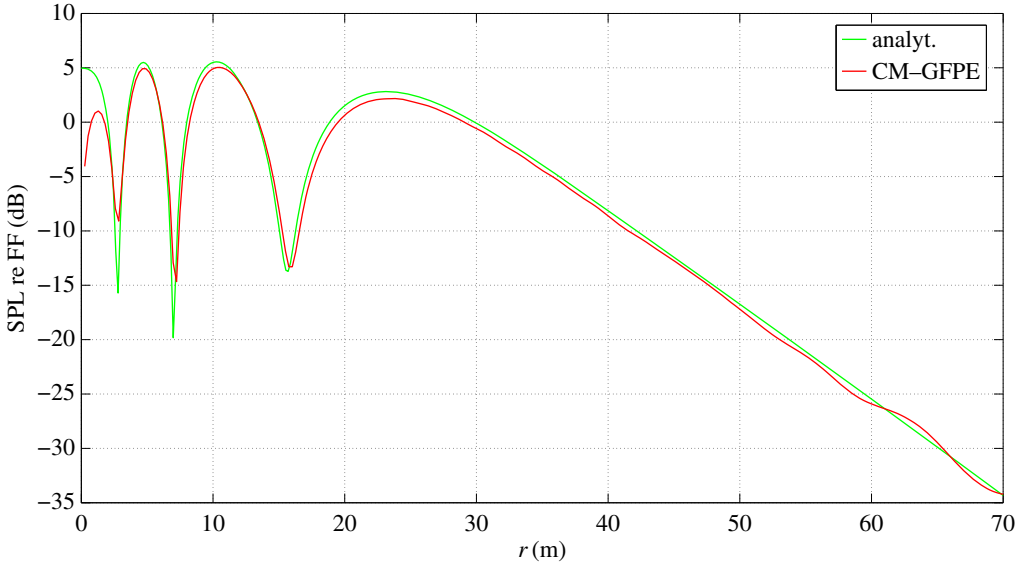

Figure 4. Sound pressure level (SPL), relative to free-field (FF) sound propagation, near a rigid convex circular cylinder at a fixed receiver height along the arc (validation case A). (Online version in colour.)

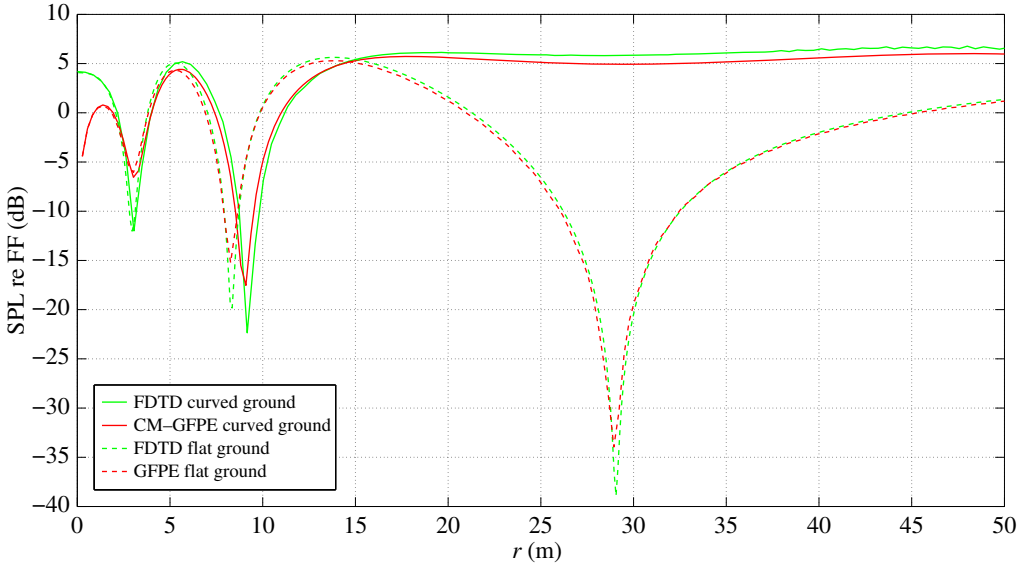

Figure 5. Sound pressure level (SPL), relative to free-field (FF) sound propagation, near a rigid concave circular cylinder at a fixed receiver height ('curved ground', validation case B) along the arc. For comparison, sound propagation over a flat rigid ground with the same source–receiver positioning is also depicted (flat ground). (Online version in colour.)

Figure 5 shows the comparison between the FDTD and the CM–GFPE methods for a concave rigid surface (validation case B). For comparison, sound propagation in the case of the same source–receiver geometry but over flat rigid ground is depicted. The specific curvature of the ground leads to some distinct effects, such as the loss of the strong destructive interference at about 29 m from the source, and the small shifts in interferences at short distance. The agreement between the FDTD and the CM–GFPE methods is very good, with differences smaller than 0.7 dB;

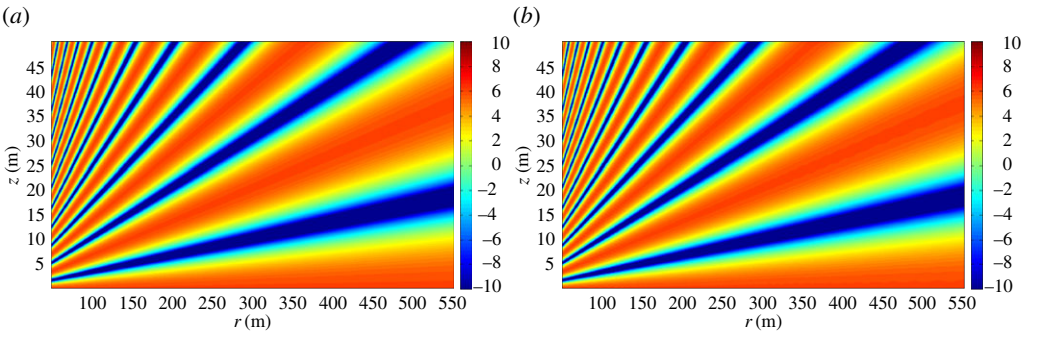

Figure 6. Sound pressure level, relative to free-field sound propagation (in dB), over flat rigid ground in a dense receiver grid. (*a*) GFPE results using an analytical starting field are depicted and (*b*) the (full) analytical solution (validation case C). (Online version in colour.)

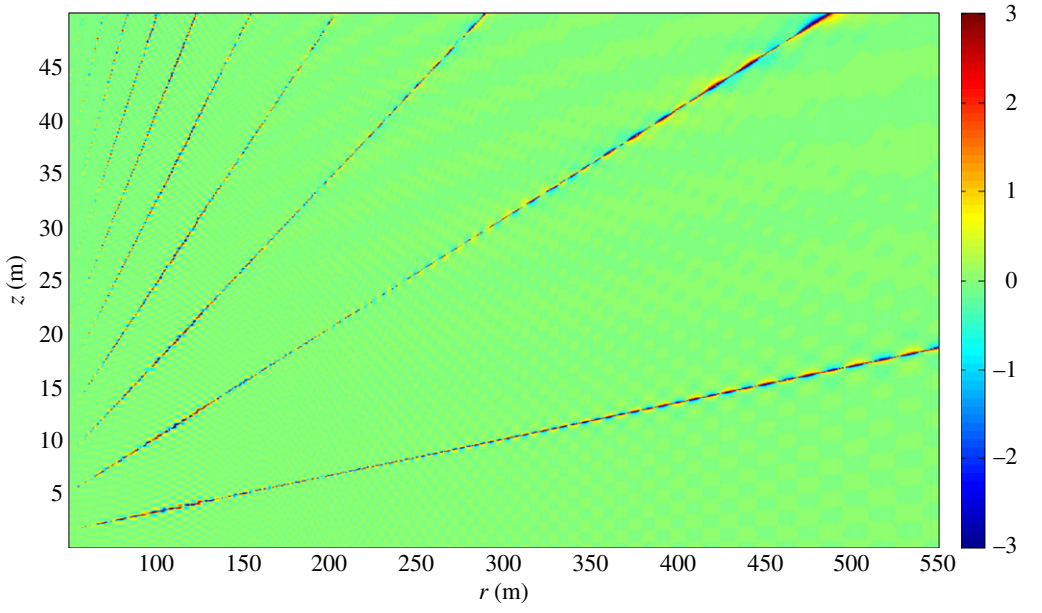

Figure 7. Sound pressure level difference (in dB) between GFPE predictions starting from an analytically constructed starting field and the full analytical solution for sound propagation over flat rigid ground (validation case C). (Online version in colour.)

similar remarks as for validation case A could be made regarding the angle limitation in PE close to the source, and regarding the magnitude of the destructive interferences. Other (small) differences might come from the fact that the FDTD is a full-wave technique, including backward scattering which is fully neglected in the forward-stepping GFPE approach, from the stair-step approach in FDTD, and from the fact that there will be small phase errors that are inherent to the FDTD technique [34]. Validation cases A and B further show the accuracy of the equivalence between a point source and coherent line source solutions in such complex geometries when expressing results relative to free-field sound propagation (see §2*a*).

Validation case C (figures 6 and 7) shows excellent agreement between the analytical solution applied to a dense receiver grid and the analytical starter propagated further with GFPE. The analytical starter is located at 50 m from the source. Only predictions from that distance on are depicted. The field plots presented in figure 6 are almost indistinguishable. The level differences

plotted in figure 7 show some small deviations only at the zones where the conditions for destructive interference are met.

5. Calculation example: valley ground type

This section shows the potential of the proposed hybrid analytical–CM–GFPE methodology to assess sound pressure levels across a valley in the case of a single ridge wind turbine. The influence of valley ground type is studied.

Sound propagating from a point source (concentrating all the wind turbine's emitted acoustic energy at hub height) at a height $z_s = 75$ m on top of the ridge is considered. The ridge part is rigid and has a radius $R_{c1} = 10$ m. Predictions are made across the adjacent valley with a radius R_{c2} of 500 m at a fixed receiver height $z_r = 4$ m (i.e. the typical receiver height as used in noise mapping). Two valley ground types are modelled, namely rigid and grass-covered ground. For the latter, the common Delany & Bazley impedance model [35] has been used as being appropriate to model reflection from grassland and characterized by a flow resistivity of 200 kPa s m^{-2}.

The following numerical parameters were used for the simulations. An absorption layer [17] thickness of 150 wavelengths is chosen, with the ratio between dr and dz being set to 30. These choices are consistent with the guidelines presented in [26]. In order to sufficiently assess the sound field along the arc, and taking into account the strong (artificial) refraction to represent the ground curvature, 40 computational cells per wavelength were chosen in the vertical direction. As a result, the spatial step dr stays below the wavelength. The starting field is constructed in detail up to 75% of the valley radius. No accuracy loss was observed by reducing the spatial sampling while calculating the starting field to five cells per wavelength, followed by linear interpolation. Part of a Hanning window was used to gradually allow the pressure to go to zero towards the top of the calculation domain in order to prevent spurious reflections. Analysis is performed in octave bands. Twenty sound frequencies were individually simulated with the hybrid analytical–CM–GFPE model to constitute each band.

Numerical results depicted in figure 8 show a rather complex sound pressure level distribution along the valley. In both ground type scenarios, significant shielding is observed directly near the source side of the valley. However, strong differences are predicted further across the valley. Starting from about the centre of the valley, near-free-field sound propagation is predicted at all octave bands for the rigid ground, while there is a much stronger reduction along the grass-covered valley. Effects become increasingly pronounced with increasing sound frequency, consistent with the fact that surface impedance decreases with frequency. These numerical simulations indicate the importance of ground type in the case of ridge wind turbines emitting sound into a valley. This behaviour deviates from wind turbine sound propagation above flat ground, where the effects of ground type are typically much less pronounced [36].

An estimation of the total wind turbine received sound pressure level is shown in figure 9, for both ground types. A (relative) spectrum is considered to allow balancing the importance of the different octave bands, as they behave quite differently during propagation across the valley. To perform this analysis, the mean over a large set of spectral source power level measurements near large horizontal-axis wind turbines with a power production of more than 2 MW, as reported in [15], is used. This spectrum is repeated in appendix B.

When assuming a total sound power level of 105 dBA, the 35 dBA broadband exposure level (i.e. −70 dBA in figure 9) below which negative noise-related effects are not expected (see Introduction) is predicted after 240 m (28°, relative to the interface between the ridge and valley segments) and 662 m (76°) propagation across the valley, for grass-covered and rigid ground, respectively. Note that these predicted distances involve a single wind turbine only; a series of wind turbines positioned on a ridge would be common practice, however.

Note that, in this assessment, the specific noise emission characteristics of wind turbines located on ridges is not included, neither are the complex wind fields that might be expected at such locations. In a strongly simplified approach, a logarithmic wind speed profile (homogeneous atmosphere) is assumed following the valley terrain, using an aerodynamic roughness length of

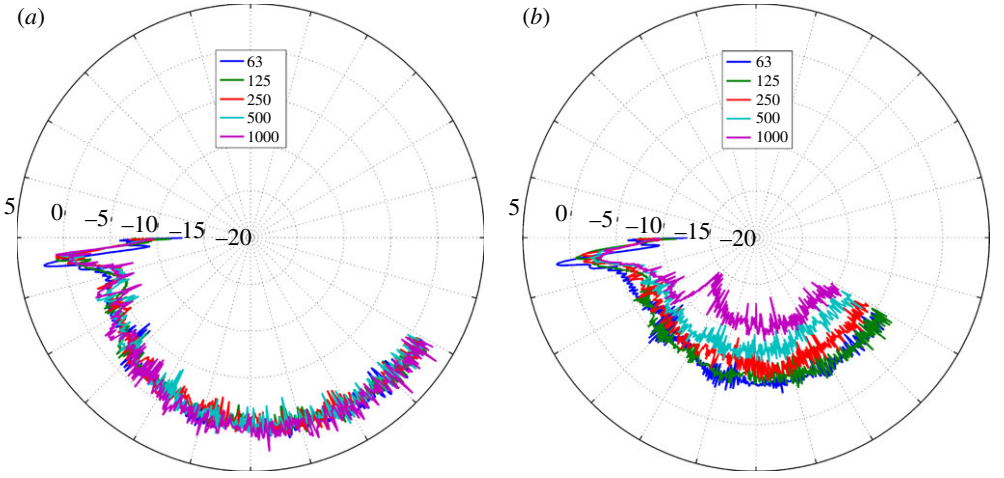

Figure 8. Predicted sound pressure levels (relative to free-field sound propagation, in dB) across the valley, in the case of a rigid (*a*) and a grass-covered valley (*b*), at a receiver height of 4 m. Octave bands with centre frequencies ranging from 63 Hz to 1 kHz are presented. (Online version in colour.)

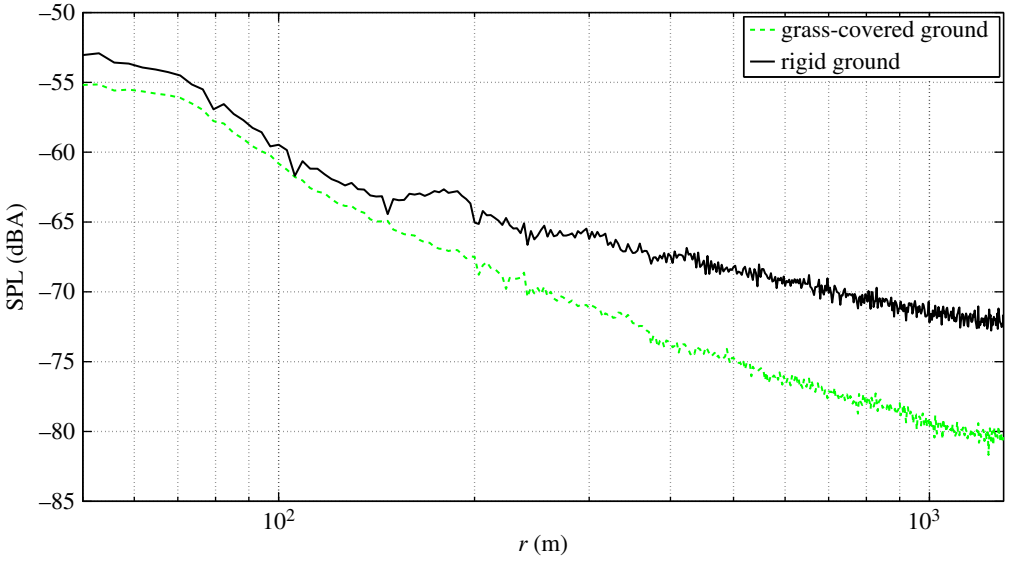

Figure 9. Predicted sound pressure levels (SPL) at a receiver height of 4 m across the valley arc, in the case of rigid and grass-covered valley ground. The total source power level is normalized to 0 dBA (see appendix B). (Online version in colour.)

0.05 m and a friction velocity of 0.4 m s^{-1}. Atmospheric absorption [37] is modelled assuming an air temperature of 10°C, a relative humidity of 70% and an atmospheric pressure of 101 300 Pa. The frequency range considered includes the octave band with centre frequency 2 kHz. For reasons of computational efficiency, the very time-consuming sound propagation calculations for the 2 kHz octave band were not performed (and the 1 kHz band results were recycled). This is justified by the fact that atmospheric absorption becomes pronounced at these higher frequencies and source power levels start to drop; a more accurate assessment of the propagation at this band would, therefore, only slightly increase accuracy when assessing total noise exposure levels from the wind turbine.

6. Conclusion

A hybrid analytical–CM–GFPE methodology is presented to model sound propagation from a ridge-mounted wind turbine, represented here by an elevated point source above the ridge, across an adjacent valley. The hybrid method relies on an analytical solution for sound diffraction around an impedance cylinder and the CM–GFPE technique. The geometry is simplified to a convex segment with a small radius, representing the ridge, followed by a large-radius concave circular segment, representing the valley. The hybrid model overcomes issues such as the unrealistic positioning of the source that would otherwise result from the CM approach, and the general angle limitation of the PE method. Various aspects of the model were successfully validated by means of cross-validations against other numerical or analytical techniques. Calculation examples show the complex sound pressure level distribution in such a ridge–valley geometry. At the source side of the valley, noise shielding from a (single) wind turbine is predicted. Starting from the centre of the valley, near-free-field sound propagation is observed at all octave bands for the rigid ground case, while there is a strong level reduction along a grass-covered valley. Although wind speed profiles were highly idealized in this work, the calculation methodology has the potential to include the effect of refraction and turbulent scattering as a result of the complex flow fields that might be associated with such a wind turbine placement.

Competing interests. I have no competing interests.
Funding. I received no funding for this study.
Acknowledgement. I am grateful to Dr Andrew Bullmore for proofreading the manuscript.

Appendix A. Analytical solution for coherent line source diffraction around an impedance cylinder

The total pressure p at point P, at a (radial) distance R relative to the origin of the cylinder, emitted by a coherent line source at point Q, parallel to the cylinder axis and at a distance R_q from the origin of the cylinder, consists of the direct contribution from Q to P ($=p_\mathrm{d}$), and the scattered sound pressure ($=p_\mathrm{s}$) [33] (see figure 10):

$$p = p_\mathrm{d} + p_\mathrm{s}. \tag{A 1}$$

The direct contribution is calculated as follows (assuming a unity-amplitude source):

$$p_\mathrm{d} = H_0^2\left(k_0\sqrt{R_\mathrm{q}^2 + R^2 - 2R_\mathrm{q}R\cos(\theta)}\right). \tag{A 2}$$

Calculating the scattered field is somewhat more involved, and needs the following summation:

$$p_\mathrm{s} = \sum_{m=0}^{\infty} a_m \delta_m J_m(k_0 R_q) H_m^2(k_0 R)\cos(m\theta) \tag{A 3}$$

with

$$\delta_m = \begin{cases} 1, & m = 0, \\ 2, & m > 0. \end{cases} \tag{A 4}$$

The term a_m in equation (A 3) is calculated as follows:

$$a_m = -\frac{\mathrm{i}J_m'(k_0 a) + (1/Z)J_m(k_0 a)}{\mathrm{i}H_m'^2(k_0 a) + (1/Z)H_m^2(k_0 a)}\frac{H_m^2(k_0 R_q)}{J_m(k_0 R_q)}. \tag{A 5}$$

The derivatives of the Bessel and Hankel functions, with respect to their arguments, can be calculated using the following expressions:

$$J_m'(k_0 a) = \frac{m}{k_0 a}J_m(k_0 a) - J_{m+1}(k_0 a) \tag{A 6}$$

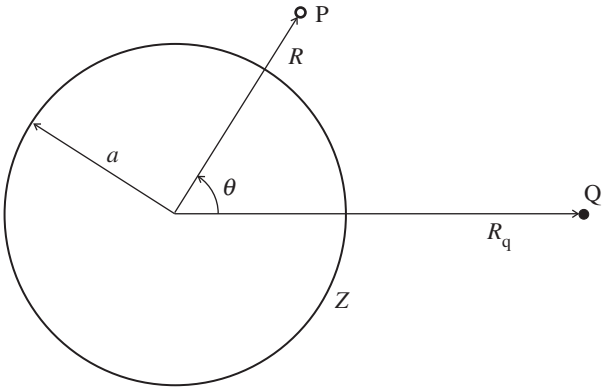

Figure 10. Overview of parameters involved in the analytical solution for coherent line source diffraction around an impedance cylinder.

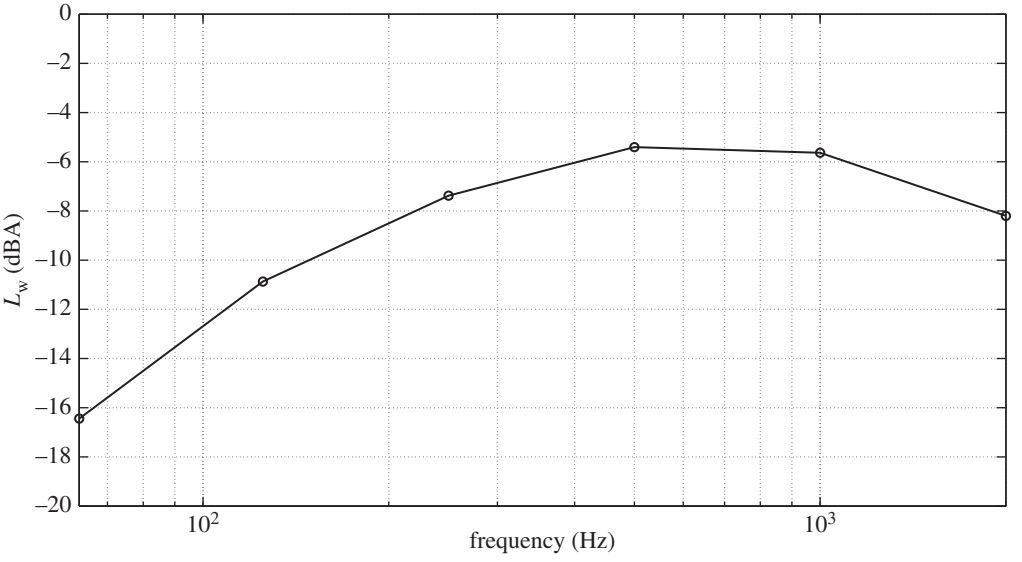

Figure 11. Source power level spectrum used for the calculations depicted in figure 9, based on Søndergaard [15]. The spectrum was normalized to a total source power level of 0 dBA.

and

$$H_m'^2(k_0a) = \tfrac{1}{2}(H_{m-1}^2(k_0a) - H_{m+1}^2(k_0a)). \tag{A 7}$$

In the equations above, k_0 is the wavenumber, a the cylinder radius, θ the angle between source and receiver, H_m^2 the Hankel function of mth order and second kind, J_m the Bessel function of order m and Z the (normalized) locally reacting surface impedance of the cylinder.

Appendix B. Wind turbine source power spectrum

The source power level spectrum depicted in figure 11 was used to calculate total A-weighted exposure levels. This spectrum is the average based on a large number of measurements near horizontal-axis wind turbines with a power production of more than 2 MW, as reported by Søndergaard [15].

References

1. Tabassum-Abbasi M, Abbasi T, Abbasi S. 2014 Wind energy: increasing deployment, rising environmental concerns. *Renew. Sust. Energy Rev.* **31**, 270–288. (doi:10.1016/j.rser.2013.11.019)
2. Kim H, Lee S, Son E, Lee S, Lee S. 2012 Aerodynamic noise analysis of large horizontal axis wind turbines considering fluid–structure interaction. *Renew. Energy* **42**, 46–53. (doi:10.1016/j.renene.2011.09.019)
3. Pedersen E, Waye K. 2004 Perception and annoyance due to wind turbine noise—a dose–response relationship. *J. Acoust. Soc. Am.* **116**, 3460–3470. (doi:10.1121/1.1815091)
4. Pedersen E, Waye K. 2007 Wind turbine noise, annoyance and self-reported health and well-being in different living environments. *Occup. Environ. Med.* **64**, 480–486. (doi:10.1136/oem.2006.031039)
5. Shepherd D, McBride D, Welch D, Dirks K, Hill E. 2011 Evaluating the impact of wind turbine noise on health-related quality of life. *Noise Health* **13**, 333–339. (doi:10.4103/1463-1741.85502)
6. Janssen S, Vos H, Eisses A, Pedersen E. 2011 A comparison between exposure–response relationships for wind turbine annoyance and annoyance due to other noise sources. *J. Acoust. Soc. Am.* **130**, 3746–3753. (doi:10.1121/1.3653984)
7. Bolin K, Nilsson M, Khan S. 2010 The potential of natural sounds to mask wind turbine noise. *Acta Acust. Acust.* **96**, 131–137. (doi:10.3813/AAA.918264)
8. Van Renterghem T, Bockstael A, De Weirt V, Botteldooren D. 2013 Annoyance, detection and recognition of wind turbine noise. *Sci. Total Environ.* **456–457**, 333–345. (doi:10.1016/j.scitotenv.2013.03.095)
9. Wharton S, Newman J, Qualley G, Miller W. 2015 Measuring turbine inflow with vertically-profiling lidar in complex terrain. *J. Wind Eng. Ind. Aerodyn.* **142**, 217–231. (doi:10.1016/j.jweia.2015.03.023)
10. Hunt J, Leibovich S, Richards K. 1988 Turbulent shear flows over low hills. *Q. J. R. Meteorol. Soc.* **114**, 1435–1470. (doi:10.1002/qj.49711448405)
11. Lemelin R, Surry D, Davenport A. 1988 Simple approximations for wind speed-up over hills. *J. Wind Eng. Ind. Aerodyn.* **28**, 117–127. (doi:10.1016/0167-6105(88)90108-0)
12. Lubitz W, White B. 2007 Wind-tunnel and field investigation of the effect of local wind direction on speed-up over hills. *J. Wind Eng. Ind. Aerodyn.* **95**, 639–661. (doi:10.1016/j.jweia.2006.09.001)
13. Evans T, Cooper J. 2011 Comparison of predicted and measured wind farm noise levels and implications for assessments of new wind farms. In *Proc. of ACOUSTICS 2011*, Gold Coast, Australia. See http://www.acoustics.asn.au/conference_proceedings/AAS2011/papers/p30.pdf.
14. Schmidt J, Klokker M. 2014 Health effects related to wind turbine noise exposure: a systematic review. *PLoS ONE* **9**, e114183. (doi:10.1371/journal.pone.0114183)
15. Søndergaard B. 2014 Noise and low frequency noise from wind turbines. In *Proc. of Internoise 2014*, Melbourne, Australia. See http://www.acoustics.asn.au/conference_proceedings/INTERNOISE2014/papers/p991.pdf.
16. Keith S, Feder K, Voicescu S, Soukhovtsev V, Denning A, Tsang J, Broner N, Richarz W, van den Berg F. 2016 Wind turbine sound power measurements. *J. Acoust. Soc. Am.* **139**, 1431–1435. (doi:10.1121/1.4942405)
17. Salomons E. 2001 *Computational atmospheric acoustics*. Dordrecht, The Netherlands: Kluwer.
18. Ostashev V, Wilson D. 2016 *Acoustics in moving inhomogeneous media*, 2nd edn. Boca Raton, FL: CRC Press.
19. Gilbert K, Di X. 1993 A fast Green's function method for one-way sound propagation in the atmosphere. *J. Acoust. Soc. Am.* **94**, 2343–2352. (doi:10.1121/1.407454)
20. Salomons E. 1998 Improved Green's function parabolic equation method for atmospheric sound propagation. *J. Acoust. Soc. Am.* **104**, 100–111. (doi:10.1121/1.423260)
21. Van Renterghem T, Salomons E, Botteldooren D. 2005 Efficient FDTD-PE model for sound propagation in situations with complex obstacles and wind profiles. *Acta Acust. Acust.* **91**, 671–679. See http://www.ingentaconnect.com/content/dav/aaua/2005/00000091/00000004/art00006/.
22. Sack R, West M. 1995 A parabolic equation for sound propagation in two dimensions over any smooth terrain profile: the generalised terrain parabolic equation (GT-PE). *Appl. Acoust.* **45**, 113–129. (doi:10.1016/0003-682X(94)00039-X)

23. Collins M. 1990 The rotated parabolic equation and sloping ocean bottoms. *J. Acoust. Soc. Am.* **87**, 1035–1037. (doi:10.1121/1.398829)
24. Bérengier M, Gauvreau B, Blanc-Benon P, Juvé D. 2003 Outdoor sound propagation: a short review on analytical and numerical approaches. *Acta Acust. Acust.* **89**, 980–991. See http://www.ingentaconnect.com/content/dav/aaua/2003/00000089/00000006/art00009/.
25. Van Renterghem T, Botteldooren D, Lercher P. 2007 Comparison of measurements and predictions of sound propagation in a valley-slope configuration in an inhomogeneous atmosphere. *J. Acoust. Soc. Am.* **121**, 2522–2533. (doi:10.1121/1.2717765)
26. Cooper J. 2003 Parameter selection in the Green's function parabolic equation for outdoor sound propagation over varied terrain. PhD thesis, Pennsylvania State University, USA.
27. Di X, Gilbert K. 1994 The effect of turbulence and irregular terrain on outdoor sound propagation. In *Proc. of the 6th Int. Symp. on Long-Range Sound Propagation*, Ottawa, Canada, pp. 315–333. National Research Council of Canada.
28. Li K, Wang Q, Attenborough K. 1998 Sound propagation over convex impedance surfaces. *J. Acoust. Soc. Am.* **104**, 2683–2691. (doi:10.1121/1.423852)
29. Defrance J *et al.* 2007 Outdoor sound propagation reference model developed in the European Harmonoise project. *Acta Acust. Acust.* **93**, 213–227. See http://www.ingentaconnect.com/content/dav/aaua/2007/00000093/00000002/art00005/.
30. Cooper J, Swanson D. 2007 Parameter selection in the Green's function parabolic equation. *Appl. Acoust.* **68**, 390–402. (doi:10.1016/j.apacoust.2006.02.008)
31. Botteldooren D. 1995 Finite-difference time-domain simulation of low-frequency room acoustic problems. *J. Acoust. Soc. Am.* **98**, 3302–3308. (doi:10.1121/1.413817)
32. Attenborough K, Li K, Horoshenkov K. 2007 *Predicting outdoor sound*. London, UK: Taylor and Francis.
33. Mechel F. 2008 *Formulas of acoustics*, 2nd edn. Berlin, Germany: Springer.
34. Van Renterghem T, Botteldooren D. 2007 Prediction-step staggered-in-time FDTD: an efficient numerical scheme to solve the linearised equations of fluid dynamics in outdoor sound propagation. *Appl. Acoust.* **68**, 201–216. (doi:10.1016/j.apacoust.2005.10.003)
35. Delany M, Bazley E. 1970 Acoustical properties of fibrous absorbent materials. *Appl. Acoust.* **3**, 105–116. (doi:10.1016/0003-682X(70)90031-9)
36. Sims J, Bullmore A, Van Renterghem T, Horoshenkov K. 2015 Wind turbine noise propagation—results of numerical modelling techniques to investigate specific scenarios. In *Proc. 6th Int. Conf. on Wind Turbine Noise*, Glasgow, UK. Institute of Noise Control Engineering.
37. ISO. 1996 *Acoustics—attenuation of sound during propagation outdoors—part 1*. ISO 9613-1:1996. Geneva, Switzerland: International Organisation for Standardisation.